Draft version December 17, 2014
Preprint typeset using LaTeX style emulateapj v. 04/17/13

RADIO SOURCES IN THE CENTRAL FILAMENT OF THE SERPENS SOUTH PROTOCLUSTER

Authors

ABSTRACT

We present 4.14 and 6.31 centimeter continuum observations of the Serpens South protocluster with the Karl G. Jansky Very Large Array in its C configuration. Our focus is a 4' x 4' area around the central filament ($\alpha = 18^{\rm h}30^{\rm m}05.00^{\rm s}, \delta = -02°02'30.0''$, J2000.0). We detect roughly 18 sources, 10 of which are probably protostellar in nature. We characterize the radio emission and put it in context with 2MASS, Spitzer and Herschel data from the region. We find new embedded protostars that have yet to be resolved at shorter wavelengths, and in some cases confirm compact centimeter emission in previously labeled starless cores. We compare our radio sources to the known centimeter vs. bolometric luminosity relationship. With our relatively short integration time and weak detection of many more possible radio sources, we speculate that longer, higher resolution radio measurements of the region would yield confident detections of many more radio protostars.

1. INTRODUCTION

Serpens South is a young stellar cluster that is a part of the broader Aquila Rift extinction feature. It lies south of the Serpens Main cloud and is just West of the bright W40 HII region. Discovered in 2008 by Gutermuth et al. (2008) as a part of the Spitzer Space Telescope's Gould Belt Legacy survey, Serpens South has been found to harbor an unusually high ratio of Class I to Class II protostars suggesting it is in a very early phase of cluster formation. Since its discovery, it has become the center of a wide range of scholarship. This has consisted of near, mid and far infrared mappings with Spitzer and Herschel tracing heated dust around protostars (Gutermuth et al. 2008; Bontemps et al. 2010), millimeter mappings with MAMBO on the IRAM 30-meter tracing cold dust (Maury et al. 2011), near infrared polarimetry revealing the importance of global magnetic fields in the cluster's formation history (Sugitani et al. 2011), molecular outflows studies (Nakamura et al. 2011; Teixeira et al. 2012), and a wealth of spectral line surveys probing filamentary infall (Kirk et al. 2013; Friesen et al. 2013; Tanaka et al. 2013; Fernández-López et al. 2014; Nakamura & Li 2014). X-ray studies of Serpens South have yet to be published. Presently only one radio study of Serpens South has been conducted, which used the VLA in its A configuration in 2011 (Ortiz-Leon et al. in prep).

Because of its isolated formation, Serpens South presents a unique opportunity to study the environmental influences on protostars in a young stellar cluster. A multi-wavelength approach will be key to fully understanding to non-normative behaviors of protostars in a high-density environment such as Serpens South.

The VLA has been a proven tool in searching for and detecting radio emission around protostars since the early 1990s (e.g., Curiel et al. 1989; Anglada et al. 1998; Reipurth et al. 1999; Beltrán et al. 2001; Eiroa et al. 2005; Shirley et al. 2007; Rodríguez et al. 2010). Early radio studies of protostars found an excess of radio emission in comparison to the Lyman-Alpha continuum drop off expected from a normal ZAMS star. Theory and observations have best explained protostellar radio emission as having two components, thermal and non-thermal. Thermal radio emission is generally assumed to be free-free emission created from an HII region. High mass protostars have a high enough internal luminosity to support a compact or ultra-compact HII region, however, low mass protostars do not. HII regions surrounding low-mass protostars are created from thermal jets that shock the material surrounding the protostar. Non-thermal emission around low and high mass protostars is still not clearly understood; it is thought to come from gyrosynchrotron emission or possibly from jets that produce synchrotron emission in their tails.

Towards the two goals of 1) locating new embedded protostars in the Serpens South protocluster and 2) better understanding the mechanisms of protostellar radio emission on a global scale, we carried out EVLA observations of Serpens South's central filament at 4.1 and 6.3 centimeters. In §2 we present our observations. In §3 we present our results. In §4 we discuss the implications of our study and in §5 we summarize our results.

1.1. *Distance to Serpens South*

The distances to Serpens South, W40 and the Serpens Main cloud are not agreed upon in the literature. When Serpens South was discovered in 2008, a distance of 260 pc ± 37 pc was adopted based on evidence that its LSR velocities matched LSR velocities of the Serpens Main cloud, which was then thought to be a part of the larger Aquila Rift extinction feature estimated to lie at 260 pc (Straižys et al. 2003). However, VLBA parallax measurements conducted in 2010 have established the distance to the Serpens Main cloud as 429 ± 2 pc (Dzib et al. 2011), meaning that Serpens Main is distinct from the the Aquila Rift if Aquila is to have a distance of 260 pc.

Gutermuth et al. (2008) also argued that Serpens South lies in front of W40, claiming that it is seen in absorption against emission from W40. If we are to follow the initial LSR velocity analysis by Gutermuth et al. (2008), we would equate Serpens South to Serpens Main and say Serpens South lies at approximately 429 pc, while W40 lies further away. Indeed, recent radio and x-ray studies adopt a distance of 600 pc to W40, although they admit the distance is poorly constrained (Kuhn et al. 2010; Rodríguez et al. 2010). Here, we adopt a distance of 429 pc for Serpens South, although we comment on how a 260 pc distance estimate would change

TABLE 1
EVLA Image Properties

Wavelength (cm)	Beam Size[a] (arcsec x arcsec)	Position Angle (degrees)	Image RMS (μJy beam^{-1})
6.31	4.8 x 3.9	13.4	11.1
4.14	3.2 x 2.5	12.7	8.5

[a] Deconvolved with robust weighting, *robust*=0.5 (Briggs 1995).

our analysis.

2. OBSERVATIONS

We observed Serpens South on July 2, 2013, for 1 hour with the EVLA in its C array configuration. The increased bandwidth of the EVLA allowed us to split our C band observation into two subbands centered at 4.75 GHz (6.31 cm) and 7.25 GHz (4.14 cm), with a bandwidth of 1.024 GHz for each subband. We focused on a 3.5 arcsec x 3.5 arcsec region around Serpens South's central filament, with a phase center positioned at α(J2000) = $18^{\rm h}30^{\rm m}05.00^{\rm s}$, δ(J2000) = $-02°02'30.0''$. Gain calibrations were done by switching to J1804 + 0101 every 10 minutes during our hour-long observation. Figure 1 shows Serpens South at 350 micron and outlines our field of view.

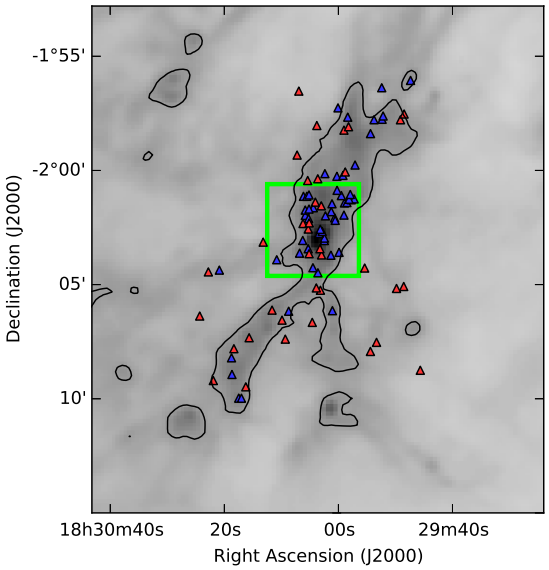

Fig. 1.— Herschel SPIRE 350 μm greyscale image of Serpens South. Blue and red triangles indicate Spitzer identified Class I and Class II protostars respectively. The green box indicates our region of interest with the EVLA.

We manually flagged, calibrated and imaged our data with standard procedures using Common Astronomy Software Applications (CASA) 4.1.0. We used J1331+305 (3C286) as a flux and bandpass calibrator, and J1804+0101 as a gain and phase calibrator ($S_{6.31\rm cm}$ = 0.70 ± 0.02 Jy, $S_{4.14\rm cm}$ = 0.66 ± 0.02 Jy). We deconvolved the Stokes I images with the Cotton-Schwab algorithm (Schwab 1984) using the CLEAN method (Högbom 1974; Clark 1980). We experimented with natural, robust and uniform weighting, and found the best compromise between noise level and source resolution with robust weighting, also known as Briggs weighting (Briggs 1995), with a *robust* parameter set to 0.5. The synthesized beam sizes and RMS values for our two images are detailed in Table 1. We also deconvolved the Stokes V images, but did not find any significant signal.

Observing Serpens South at radio wavelengths is difficult because of the extended and bright HII region W40 directly to the East, which adds to over-resolved flux and increases the RMS noise level in our images. In addition, our short integration time–45 minutes on source–left us with a less than desirable UV coverage at long UV distances. Long UV distance coverage is particularly important because we are trying to resolve point source emission. Further EVLA studies of Serpens South would benefit from extended array configurations and longer integration times.

3. RESULTS

3.1. *Radio Source Selection*

In choosing our sources, we restricted ourself to a circular region centered on our phase center and extending out to 50% of the primary beam strength. We chose our sources based on their strength in our 4.1 and 6.3 cm maps, their possible spatial alignment with infrared sources, and by referencing a source extracted sample using Sextractor (Bertin & Arnouts 1996). We took only sources that had at least a 4σ strength in the 4.1 cm image, and were left with a total of 18 radio sources. We note that we found ∼6 sources at the 2σ level that aligned within 2 arcsecond of an infrared association, however, we do not consider them strong detections and do not include them in our final source list. As stated in section 2, further observations with longer integration will likely be able to confidently detect these protostellar radio sources.

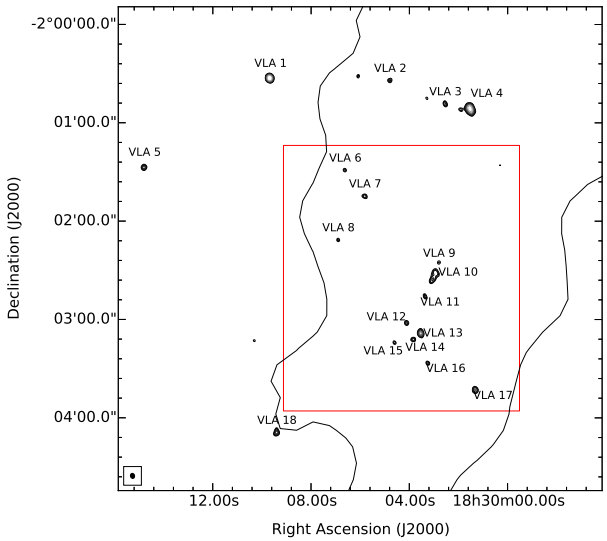

Fig. 2.— Serpens South radio continuum at 6.3 cm, focused in on green box from Figure 1. Radio contours start at 4σ and end at 50σ. The loose black contour is the same SPIRE 350 μm contour found in Figure 1.

We ran source extractions on the spatial positions of our final source list over the JHK bands of 2MASS, the four IRAC bands of Spitzer, the 24 μm MIPS band on

TABLE 2
RADIO PROPERTIES OF VLA SOURCES

Source	RA[a] (J2000)	Decl.[a] (J2000)	$S^{int}_{6.3cm}$ [b] (μJy)	$S^{peak}_{6.3cm}$ (μJy beam^{-1})	$S^{int}_{4.1cm}$ (μJy)	$S^{peak}_{4.1cm}$ (μJy beam^{-1})	α^{int}_{radio}	α^{peak}_{radio}	Class[e]
VLA_1	18 30 09.68	-02 00 32.8	749 ± 6	718	844 ± 8	794	0.28 ± 0.01	0.24 ± 0.02	Extragal.?
VLA_2	18 30 04.79	-02 00 34.1	177 ± 7	138	87 ± 7	72	-1.67 ± 0.09	-1.55 ± 0.14	Extragal.
VLA_3	18 30 02.55	-02 00 48.5	140 ± 2	99	116 ± 10	87	-0.46 ± 0.1	-0.3 ± 0.15	Extragal.
VLA_4	18 30 01.53	-02 00 51.6	1663 ± 32	1178	946 ± 28	515	-1.33 ± 0.04	-1.96 ± 0.02	Extragal.
VLA_5	18 30 14.79	-02 01 27.3	106 ± 5	95	167 ± 10	173	1.07 ± 0.08	1.41 ± 0.13	Extragal.?
VLA_6	18 30 06.62	-02 01 28.9	79 ± 7	61	33 ± 4	56	-2.04 ± 0.16	-0.22 ± 0.23	Extragal.
VLA_7	18 30 05.81	-02 01 44.9	48 ± 4	40	84 ± 7	63	1.29 ± 0.13	1.08 ± 0.31	Class I
VLA_8	18 30 06.89	-02 02 11.5	39 ± 3	46	50 ± 6	50	0.55 ± 0.15	0.18 ± 0.29	Extragal.?
VLA_9	18 30 02.80	-02 02 25.3	66 ± 1	50	60 ± 1	44	-0.22 ± 0.03	-0.31 ± 0.29	Class 0?
VLA_10	18 30 02.95	-02 02 32.2	287 ± 6	119	260 ± 17	73	-0.23 ± 0.07	-1.15 ± 0.15	Unknown
VLA_11	18 30 03.36	-02 02 45.8	38 ± 2	36	73 ± 4	58	1.5 ± 0.09	1.14 ± 0.34	Class 0
VLA_12	18 30 04.11	-02 03 02.1	30 ± 2	24	79 ± 2	58	2.31 ± 0.09	2.06 ± 0.48	Class 0*
VLA_13	18 30 03.54	-02 03 08.4	186 ± 1	178	231 ± 3	227	0.51 ± 0.02	0.58 ± 0.07	Class 0*
VLA_14	18 30 03.84	-02 03 12.2	31 ± 0	37	83 ± 2	61	2.29 ± 0.04	1.19 ± 0.33	Class 0*
VLA_15	18 30 04.60	-02 03 14.1	68 ± 1	52	49 ± 4	51	-0.74 ± 0.09	-0.08 ± 0.27	Extragal.
VLA_16	18 30 03.25	-02 03 26.6	63 ± 2	58	55 ± 1	65	-0.28 ± 0.04	0.27 ± 0.23	Class II
VLA_17	18 30 01.32	-02 03 42.9	146 ± 3	135	161 ± 4	167	0.22 ± 0.04	0.5 ± 0.1	Class I
VLA_18	18 30 09.40	-02 04 08.8	170 ± 3	182	167 ± 10	134	-0.04 ± 0.07	-0.71 ± 0.09	Extragal.?

[a] Centers of 2D gaussian fits for sources in 4.1 cm map, quoted in J2000 coordinates.
[b] Flux values from images deconvolved with Briggs weighting, *robust*=0.5 (Briggs 1995).
[c] Spectral index of integrated flux from 6.3 to 4.1 cm, see section 3 for details on calculation.
[d] Spectral index of peak flux from 6.3 to 4.1 cm.
[e] Classification of source. Unless otherwise noted, Class 0 classifications come from Herschel (Bontemps et al. 2010) and Class I & II from Spitzer (Gutermuth et al. 2008). (?) denotes uncertaintity. (*) denotes classified by this work.

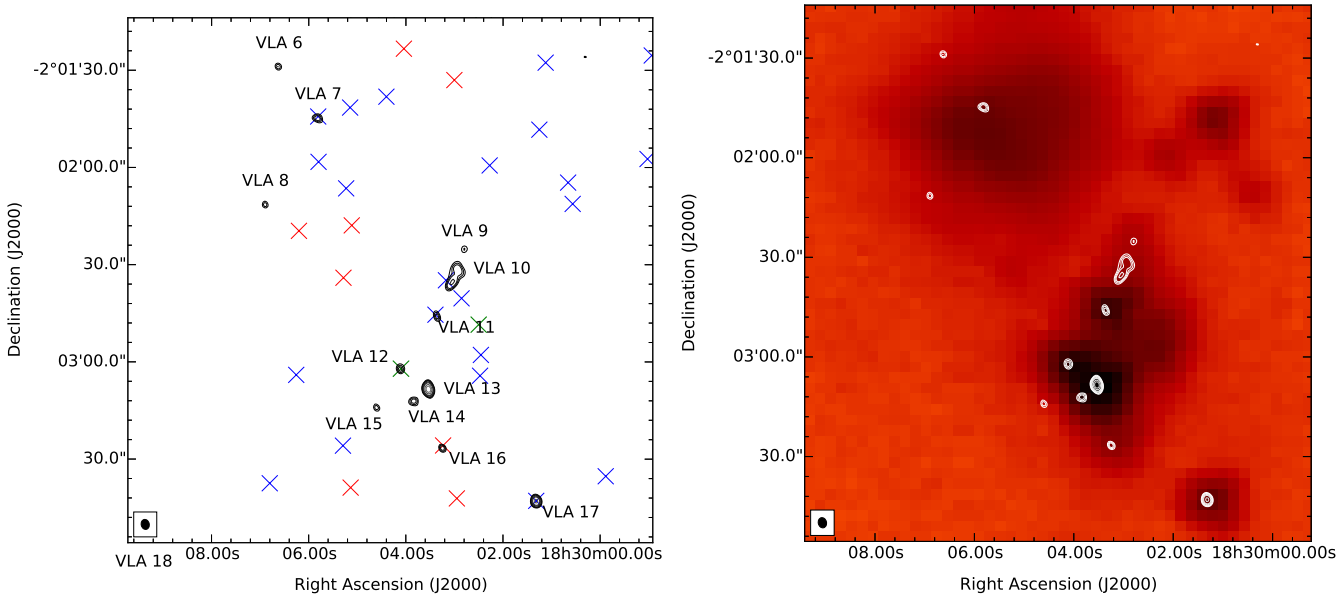

FIG. 3.— **Left**: Radio continuum at 6.3 cm focused in on red box from Figure 2. Blue and red crosses correspond to Spitzer identified Class I and II protostars. Green crosses correspond to 1.2 mm dust peaks identified by IRAM. **Right**: Identical contours on the left but with a background PACS 70 μm image. The radio contour beam size is shown to the lower-left.

Spitzer, and the 70 μm PACS band on Herschel. We used a 2 arcsecond maximum matching tolerance for these extractions. Apertures and adopted corrections were consistent with the HOPS survey.

Eight of our radio sources have at least one infrared source match from 1.25 μm to 70 μm, four of which spatially match Spitzer identified Class I/II protostars within 1 arcsecond. A total of ten out of our 18 sources have signs that indicate they are protostellar in nature. One of our radio sources, VLA 12, matches a 1.2 mm source within 1 arcsecond identified by (Maury et al. 2011), which they quote as starless.

We can calculate the number of random background sources we would expect to find in our images. We use the formulation found in Shirley et al. (2007), who draw from radio studies done by Fomalont et al. (1991). The density of random background radio sources above a flux limit of S μJy at 6 cm is given by $N(>S) = 0.42 \cdot (S/30\ \mu\text{Jy})^{-1.18}$ arcmin^{-2}. Therefore, the total number of sources with flux S greater than 50 μJy at 6 cm is 0.229 arcmin^{-2}. This leads to a 0.4% chance that a background source falls inside any one synthesized beam centered on a compact radio source, and gives us on average ~9 background sources above 50 μJy within our 3.5' x 3.5' region of interest. This agrees with our analysis, as we find roughly 8 sources that are likely background sources.

3.2. *Radio Source Classifications*

Extragalactic Sources — VLA 2, 3, 4, 6, and 15 are very likely extragalactic in nature. They have no visible associations from 1μm to 70μm and have negative radio spectral indices indicative of non-thermal synchrotron emission.

Unclear Sources — While VLA 1 and 5 have no infrared, far-infrared or millimeter associations and are isolated from the filament, they have a flat and rising radio spectral indices suggesting optically thin and thick free-free emission respectively. Although galaxies can produce free-free emission from large HII clouds, the dominant component of a galaxy's radio emission output comes from non-thermal synchrotron emission with a declining spectrum. Nonetheless, we tentatively classify these sources as extragalactic due to their lack of associations.

VLA 18 is spatially distinct from the filament but has a flat radio spectral index and actually has three very weak infrared associations at 3.6, 4.5 and 5.8 μm. However, we speculate that these associations are coincidental and tentatively classify VLA 18 as extragalactic.

We are unsure as to the nature of VLA 10. We treat the whole elongated structure as one source. At our higher resolution 4.1 cm image, we can resolve two distinct emission components that are blended at our lower resolution 6.3 cm image (Figure 4). We cannot confidently rely on our gaussian fitted fluxes or spectral index due to the morphology of the source. For VLA 10's peak flux, we used the Northern structure in the 4.1 cm map. Although our measured peak fluxes are highly uncertain due to confusion at 6.3 cm, VLA 10's peak flux derived spectral index is strongly negative suggesting non-thermal emission and an extragalactic classification. However, VLA 10's Southern structure is also within 2 arcseconds of a Spitzer identified Class I source. This raises the possibility that the Northern structure is a background source while the Southern structure is a Class I protostellar radio source.

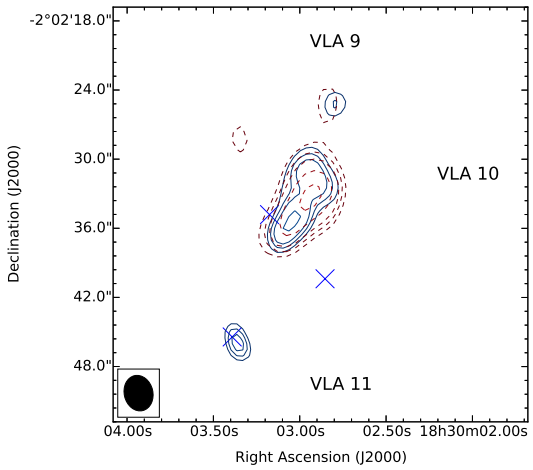

FIG. 4.— Zoom in of the elongated VLA 10 source. Blue solid and red dashed contours correspond to 4.1 and 6.3 cm images respectively. The lower-left beam is the 4.1 cm beam size. Blue crosses represent Spitzer identified Class I sources.

Another possibility is that VLA 10 is representative of an outflow shock emanating from either the Southern VLA 10 structure or from sources VLA 11 or 9. An H_2 study conducted by Teixeira et al. (2012), however, labeled VLA 11 as an outflow source with a jet running from North-East to South-West, almost perpendicular to the direction necessary for it to be an outflow source powering VLA 10's emission. Further evidence that would support a non-extragalactic classification of both the South and North structures of VLA 10 is the fact that the cold dust seen at and longward of 70 μm neatly fits around VLA 10's elongated morphology, as seen in Figure 3.

Protostellar Sources — The remainder of our 18 sources, VLA 7, 9, 11, 12, 13, 14, 16 and 17 are likely protostellar in nature. With the exception of VLA 9, all of these sources have either flat or rising radio spectral indices indicative of optically thin or thick free-free emission. We classify VLA 12, 13 and 14 as three newly identified embedded Class 0 protostars, separated form each other by less than 15 arcseconds.

4. DISCUSSION

4.1. *Protostars in the Central Filament*

Spitzer observations revealed dozens of Class I and II protostars spatially correlated to the central filament (Gutermuth et al. 2008). Herschel observations revealed colder clumps of dust corresponding to younger Class 0 protostars (Bontemps et al. 2010), however, with their poor spatial resolution they cannot reasonably resolve individual compact cores.

4.2. *$L_{infrared}$ and L_{bol} Relationship*

The internal luminosity $L_{\rm int}$ of a protostar is defined as the total luminosity from the protostar and its circumstellar disk if present. The bolometric luminosity of a source can then defined as $L_{\rm bol} = L_{\rm int} + L_{\rm ext}$, where the external luminosity comes from the heated protostellar

envelope. It is estimated that $L_{\rm ext}$ contributes to $L_{\rm bol}$ on the order of 0.1 $L_\odot$ Dunham et al. (2008) developed a scaling law relating an embedded protostar's 70 μm flux to its internal luminosity $L_{\rm int}$.

REFERENCES

Anglada, G., Villuendas, E., Estalella, R., et al. 1998, AJ, 116, 2953 [1]
Beltrán, M. T., Estalella, R., Anglada, G., Rodríguez, L. F., & Torrelles, J. M. 2001, AJ, 121, 1556 [1]
Bertin, E., & Arnouts, S. 1996, A&AS, 117, 393 [3.1]
Bontemps, S., André, P., Könyves, V., et al. 2010, A&A, 518, L85 [1, 2, 4.1]
Briggs, D. S. 1995, dissertation [1, 2, 2]
Clark, B. G. 1980, A&A, 89, 377 [2]
Curiel, S., Rodriguez, L. F., Bohigas, J., et al. 1989, Astrophysical Letters and Communications, 27, 299 [1]
Dunham, M. M., Crapsi, A., Evans, II, N. J., et al. 2008, ApJS, 179, 249 [4.2]
Dzib, S., Loinard, L., Mioduszewski, A. J., et al. 2011, in Revista Mexicana de Astronomia y Astrofisica Conference Series, Vol. 40, Revista Mexicana de Astronomia y Astrofisica Conference Series, 231–232 [1.1]
Eiroa, C., Djupvik, A. A., & Casali, M. M. 2008, The Serpens Molecular Cloud (Unpublished), 693 []
Eiroa, C., Torrelles, J. M., Curiel, S., & Djupvik, A. A. 2005, AJ, 130, 643 [1]
Fernández-López, M., Arce, H. G., Looney, L., et al. 2014, ApJ, 790, L19 [1]
Fomalont, E. B., Windhorst, R. A., Kristian, J. A., & Kellerman, K. I. 1991, AJ, 102, 1258 [3.1]
Friesen, R. K., Medeiros, L., Schnee, S., et al. 2013, MNRAS, 436, 1513 [1]
Gutermuth, R. A., Bourke, T. L., Allen, L. E., et al. 2008, ApJ, 673, L151 [1, 1.1, 2, 4.1]
Högbom, J. A. 1974, A&AS, 15, 417 [2]
Kirk, H., Myers, P. C., Bourke, T. L., et al. 2013, ApJ, 766, 115 [1]
Kuhn, M. A., Getman, K. V., Feigelson, E. D., et al. 2010, ApJ, 725, 2485 [1.1]
Maury, A. J., André, P., Men'shchikov, A., Könyves, V., & Bontemps, S. 2011, A&A, 535, A77 [1, 3.1]
Nakamura, F., & Li, Z.-Y. 2014, ApJ, 783, 115 [1]
Nakamura, F., Sugitani, K., Shimajiri, Y., et al. 2011, ApJ, 737, 56 [1]
Reipurth, B., Rodríguez, L. F., & Chini, R. 1999, AJ, 118, 983 [1]
Rodríguez, L. F., Rodney, S. A., & Reipurth, B. 2010, AJ, 140, 968 [1, 1.1]
Schwab, F. R. 1984, AJ, 89, 1076 [2]
Shirley, Y. L., Claussen, M. J., Bourke, T. L., Young, C. H., & Blake, G. A. 2007, ApJ, 667, 329 [1, 3.1]
Straižys, V., Černis, K., & Bartašiūtė, S. 2003, A&A, 405, 585 [1.1]
Sugitani, K., Nakamura, F., Watanabe, M., et al. 2011, ApJ, 734, 63 [1]
Tanaka, T., Nakamura, F., Awazu, Y., et al. 2013, ApJ, 778, 34 [1]
Teixeira, G. D. C., Kumar, M. S. N., Bachiller, R., & Grave, J. M. C. 2012, A&A, 543, A51 [1, 3.2]

APPENDIX

To Include in Paper:

– Discussion on radio spectral indices and their implications to emission

– Does optically thick radio emission from Spitzer Class I/II source mean anything particularly interesting? B/c it is Spitzer identified, does it mean that it comes not from an ultra-compact region but from some other mechanism?

– Discussion on VeLLOs in sample.

– L_int correlations?

– Make radio_alpha vs. L_bol or L_int graph?

– Fit Spitzer end of SED to get more accurate L_MIR ?

Questions:

– What does Rob say about SS distance?

– What paper should I quote for infrared source extraction photometry analysis?

– Do we have to worry about vibrational dust emission in our 4.1 cm data?

– What can we say about optically thick radio sources that match Spitzer sources? Embedded Class I source?

– Is it even physically possible for VLA 10 to be a radio galaxy outflow source? In other words, is a 10 arcsecond angular extent on the size scale of typical radio galaxy outflows?

– Can we get a table of Herschel protostars from Bontemps et al. 2010? Other papers, Teixeira12, Nakamura14 and more, quote protostellar classifications of individual protostars from Herschel data as if they had access to a

Bontemps2010 catalogue. Perhaps they just asked the authors and got access to it. Ideally, we would want a catalogue of Class 0 protostars identified by Herschel with their flux values from 250 - 500 μm, the adopted FWHM apertures in the source extraction and Lbol and Menv properties they subsequently derived.